Soliton Raman shift wavelength tuning through the pump pulse polarization control

Dmitry Korobko*[a], Ivan Panyaev[a], Pavel Itrin[a], Patrice Mégret[b], Ivan Chapalo[b] and Andrei Fotiadi[b,c]
[a]Ulyanovsk State University, 42 Leo Tolstoy Street, Ulyanovsk, 432970, Russian Federation;
[b]Electromagnetism and Telecommunication Department, University of Mons, Mons B-7000, Belgium; [c]Optoelectronics and Measurement Techniques Unit, University of Oulu, Oulu, Finland.

ABSTRACT

In addition to the well-known problem related to the growing demands in telecom fiber optical data transmission lines with extended bandwidth in recent years the researchers developed an interest in mode-locked fiber lasers of 1600-1700 nm spectral region in a number of biomedical applications. The known approach to get the generation in this range uses the Er-doped fiber mode-locked seed source of telecom range. The output ultrashort pulse then propagates in nonlinear optical fiber with anomalous dispersion undergoing the Raman shift to the longer wavelengths.

We propose a method to control the characteristics of the output Raman soliton spectrum adjusting the polarization of the pump pulse at the input of the nonlinear fiber. We have shown that this method allows to tune the wavelength of the output spectrum maximum in the whole range (1600-1700 nm) while the output power remains constant. Our simulation results agree with experimental observations.

Keywords: Raman soliton shift, extended telecom range, large mode area photonic crystal fiber

1. INTRODUCTION

Due to a wide range of applications, design of laser sources of extended telecom range is among hot topics of modern laser physics [1-5]. In addition to the well-known problem related to the growing demands in telecom fiber optical data transmission systems of extended bandwidth in recent years the researchers developed an interest to the mode-locked lasers of 1600-1700 nm spectral range for a number of biomedical applications [6-10]. This wavelength area is located in the third optical window, and defines the spectral region where the light has minimum scattering losses and a maximum depth of penetration in tissue, so these sources are in high demand in the development of biomedical multiphoton imaging system [6-10]. Laser sources operating at the wavelengths over 1.8 μm is of particular interest for applications in LIDARs, spectroscopy, and atmospheric analysis [11-14]. Passively mode-locked fiber lasers combining high beam quality, simplicity of adjustment, reliability, user-friendly fiber interface and relatively low cost are of great demand for these applications [1-17].

One of the approaches to fiber lasers developing in these wavelength regions is the application of Bismuth, Thulium or Holmium doped fibers with luminescence window in this spectral range [18-21]. Nevertheless, despite the unique optical properties of these fibers and significant achievements in their applications, the widespread use of such schemes is limited by the lower availability and higher cost of special fiber-optic components (isolators, lenses, multiplexers, semiconductor mirrors, etc.) designed for the spectral range over 1.6 microns, compared to the standard telecom range components of the same quality. The configurations based on the erbium mode-locked fiber lasers and amplifiers of the range 1540-1570 nm are free from the above-mentioned shortcomings. The output pulses of these systems injected into a final nonlinear fiber with anomalous dispersion are split into solitons that undergo Raman shift to the longer wavelengths [22-28]. The benefits of this approach are not only advanced technologies of telecom mode-locked fiber lasers, but also the possibility of simple wavelength tuning due to varying value of the Raman shift.

The parameters of the output fiber are often restricted by the requirements of special application, which declare the minimum pulse energy of about 1 nJ and more [27]. The relatively high nonlinearity of standard single-mode fibers prevents the achievement of energies in nJ range leading to mandatory application of the output fiber with low nonlinearity, for example, large mode area (LMA) photonic crystal fiber with a mode area up to 500 μm^2 or more [29-

31]. The well-known way to tune the output wavelength of the Raman solitons is to control the peak power or frequency chirp of the laser pulse at the input of the LMA fiber. The dependence of the Raman soliton energy on the value of the wavelength shift is the serious drawback of these methods particularly for multiphoton imaging applications [32-35]. An alternative way utilizing the change of the initial pulse polarization state typically relates to the output fiber with high birefringence [36-38]. Polarization rotation of the initial linearly polarized pulse at the input of the anisotropic fiber can induce the elliptical polarization of the propagating pulse leading to the different spectral shift for each of the polarization component. This method has been successfully applied in supercontinuum generation [39, 40]. The technique of combining power and polarization control in a polarization-maintaining LMA fiber can be applied to the power adjustment of the polarization components [41].

The experimental investigation of polarization tuning of soliton Raman shift in fibers with low birefringence is rather a difficult task because of the strict twisting control and minimization of external impacts are required. Some experimental results on soliton Raman shift in the low birefringent fibers pumping by linearly polarized pulses one can be found in [42]. Recent studies of soliton Raman shift evolution in an isotropic PC-rod has shown that wavelength-shifted, elliptically polarized solitons can be generated by the elliptically polarized input pulse [43]. The authors of [43] demonstrated that in order to achieve necessary wavelength of the output Raman soliton, a certain tuning of polarization state of input pulse is required. The results show that the required input pulse energy is the lowest for a linearly polarized pump pulse, and is the highest for a circularly polarized pulse.

In this paper, we consider the polarization tuning of the wavelength of Raman soliton with fixed output power in a commercially accessible LMA fiber with low birefringence. The evolution of the pulse propagating in the LMA fiber is studied numerically and experimentally through investigation of the Raman shift and output polarization depending on the polarization state of the initial pulse with fixed energy. It is established that the correct adjustment of the input pulse polarization can lead to the wavelength shift of the output Raman soliton in the targeted range of 1600–1700 nm while maintaining its energy. The output pulse with a duration of less than 100 fs and an energy of up to 10 nJ is quite enough for wide range of biomedical applications [44-48].

2. NUMERICAL SIMULATIONS

As a first step, the simulations of the pump pulse propagation in LMA fiber with low birefringence are carried out. We consider simplified approach on the base of coupled nonlinear Schrödinger equations (NSE) for polarization components derived in [49-52]. This type of the NSE takes into account higher orders of dispersion, four-wave mixing, self- and cross-phase modulation and time-delayed nonlinear response due to self- and cross-polarized Raman gain

$$\frac{\partial A_j}{\partial z} \pm \delta \frac{\partial A_j}{\partial t} - \sum_{k\geq 2}^{k=4} \frac{i^{k+1}\beta_k}{k!}\frac{\partial^k A_j}{\partial t^k} - \frac{lA_j}{2} - i\gamma\left(\left|A_j\right|^2 + \frac{2}{3}\left|A_{3-j}\right|^2\right)A_j - \frac{i\gamma}{3}A_j^* A_{3-j}^2 + \\ + i\gamma\left(\tau_1\frac{\partial\left|A_j\right|^2}{\partial t} + \tau_2\frac{\partial\left|A_{3-j}\right|^2}{\partial t}\right)A_j + i\gamma\tau_3\frac{\partial\left(A_j A_{3-j}^*\right)}{\partial t}A_{3-j} = 0, \qquad j=1,\ 2. \qquad (1)$$

Here, β_k are the dispersions (β_2 is the group velocity dispersion, β_3 is the third order dispersion, etc.), γ is the Kerr nonlinearity parameter, δ is the strength of fiber birefringence and l is the loss in the fiber. Raman response coefficients satisfy the equality $\tau_2 = \tau_3 = \tau_1/3 = 1.15$ fs. Parameter values corresponding to the typical nearly isotropic LMA silica fiber used in simulations are shown in the Table 1. We should comment that for generality we make an assumption about low but non-zero fiber birefringence δ .

Table 1. Parameters of the LMA fiber used in the simulations.

Parameter	Value	Parameter	Value
γ (W^{-1} km^{-1})	0.5	β_4 (ps^4km^{-1})	$-3\cdot10^{-4}$
β_2 (ps^2km^{-1})	-37	l (dB m^{-1})	0.3
β_3 (ps^3km^{-1})	0.15	δ (ps m^{-1})	0.01

We consider the propagation of the input pump pulse specified in the form of the *N*-soliton $A(t)=\sqrt{P_0}\,\mathrm{sech}(t/\tau)$ in the fiber with the length $L=1\,\mathrm{m}$ for different initial states of polarization defined as

$$A_1 = A_s = A\cos\theta\exp(i\varphi/2),$$
$$A_2 = A_p = A\sin\theta\exp(-i\varphi/2),$$

where θ is the polarization angle and ϕ is the phase difference between the components A_j. The duration and the peak power of the input pulse are equal to $\tau=0.45\,\mathrm{ps}$ and $P_0=22\,\mathrm{kW}$, respectively. We compare the propagation of the input pulse for circular, linear and elliptic input polarizations determined by the values of the θ and φ. These values are defined as $\theta=\pi/4$, $\varphi=\pi/2$ for circular; $\theta=0$, $\varphi=0$ for s- linear and $\theta=\pi/4$, $\varphi=\pi/8$ for one of the possible elliptic polarization states, respectively. Results of simulations of the pulse propagation for each of the polarization components are shown in Figures 1, 2.

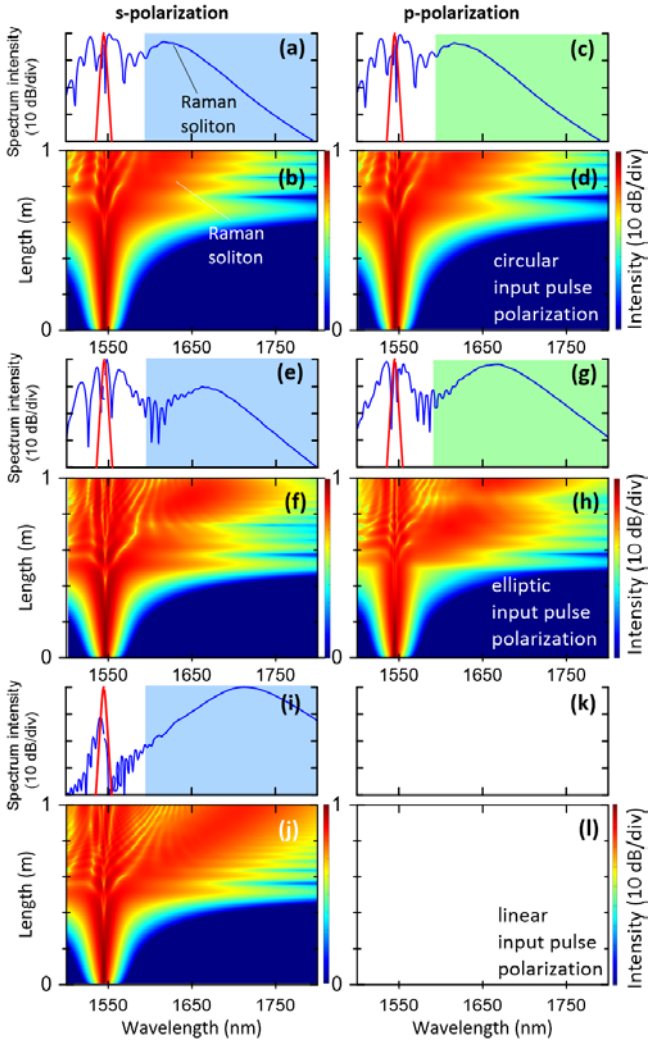

Figure 1. Propagation of the pump pulse in the LMA fiber for different initial states of polarization. Results of numerical simulations. (a, b, c, d) Circular polarization of the input pulse. Spectra at the input (red) and at the output (blue line) of the fiber for s- (a) and p- (c) polarization components. Evolution of the spectrum intensity for s- (b) and p- (d) polarization components. (e, f, g, h) The same as (a, b, c, d) but for elliptic polarization of the input pulse. (i, j, k, l) The same as (a, b, c, d) but for linear s-polarization of the input pulse. Parts of the spectra, which can pass through long-pass filter with cutoff wavelength $\lambda=1600$ nm are colored in blue (for s-) and green (for p-polarization component).

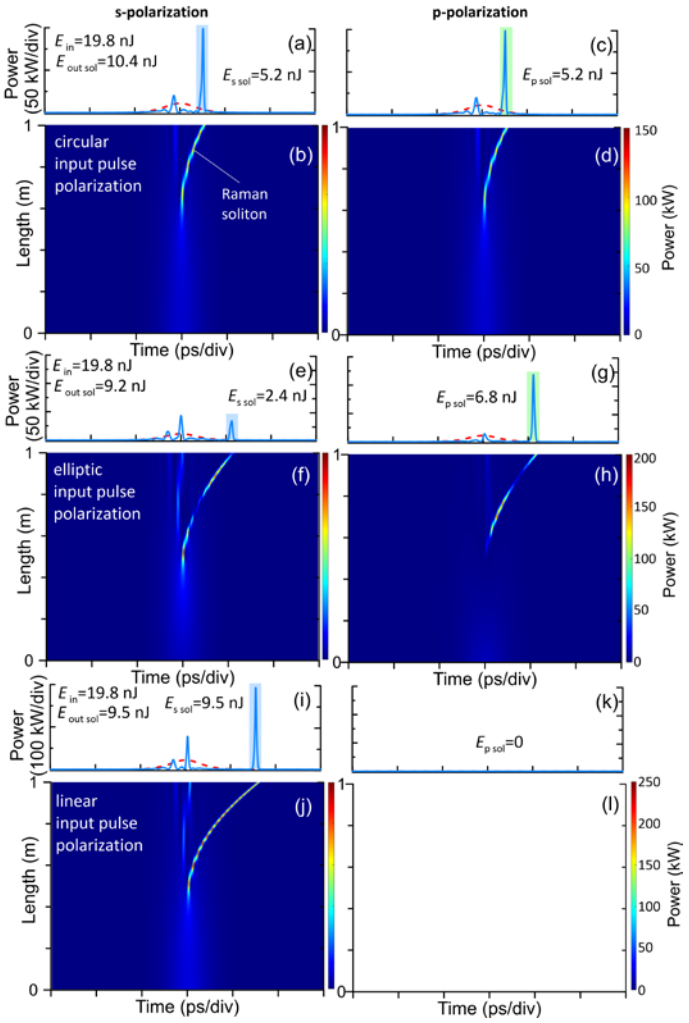

Figure 2. Propagation of the pump pulse in the LMA fiber for different initial states of polarization. Results of numerical simulations. (a, b, c, d) Circular polarization of the input pulse. Radiation intensity at the input (dashed red) and at the output (blue line) of the fiber for s- (a) and p- (c) polarization components. Evolution of the radiation intensity for s- (b) and p- (d) polarization components. (e, f, g, h) The same as (a, b, c, d) but for elliptic polarization of the input pulse. (i, j, k, l) The same as (a, b, c, d) but for linear s-polarization of the input pulse. Raman solitons are colored in blue (for s-) and green (for p-polarization component). Energies of the pump pulse (E_{in}) and Raman solitons ($E_{out\ sol}$ – is the total energy, $E_{s\ sol}$, $E_{p\ sol}$ – are the energies of s- and p-polarization components of the Raman soliton) are also shown.

Ultimately, the evolution of the circularly polarized pump pulse provokes the formation of the Raman soliton with peak power and energy equal for both polarizations. Otherwise, the linearly polarized Raman soliton of maximum peak power is achieved due to linearly polarized pump pulse. The pump pulse with elliptic input polarization can be considered as transition between these extreme states leading to generation of Raman soliton consisting from two coupled polarization components. The peak power of the higher energy component of elliptically polarized Raman soliton is intermediate between the peak powers of linearly and circularly polarized Raman solitons. As a result, we can see that the nonlinear Raman wavelength shift, which is minimal for the circularly polarized pump pulse, increases for the elliptically polarized and reaches the maximum for the linearly polarized pump pulse.

Figure 2 shows the simulation data dealing with the energy of the initial pump pulse and energies of s- and p-components of Raman soliton at the fiber output. As can be seen, conversion of the pump pulse energy into the energy of output Raman soliton is about 45-55% with maximum level corresponding to the circular polarization of the input pulse.

At the same time, one should note that the application of long-pass filter could control the output pulse energy. Considering the long-pass filter with cutoff wavelength $\lambda = 1600$ nm (Figure 1) we conclude that the linearly and elliptically polarized Raman solitons can freely pass through the filter but some part of the energy of circularly polarized soliton can be lost on it. Therefore, appropriate tuning of the long-pass filter allows to decrease the change in output energy of Raman solitons and to build the generator of Raman solitons with the energy approximately independent on the wavelength. Raman shifts obtained for the circularly and linearly polarized input pulses determine the limits of wavelength tuning that could be performed by polarization adjustment of the pump.

3. EXPERIMENT

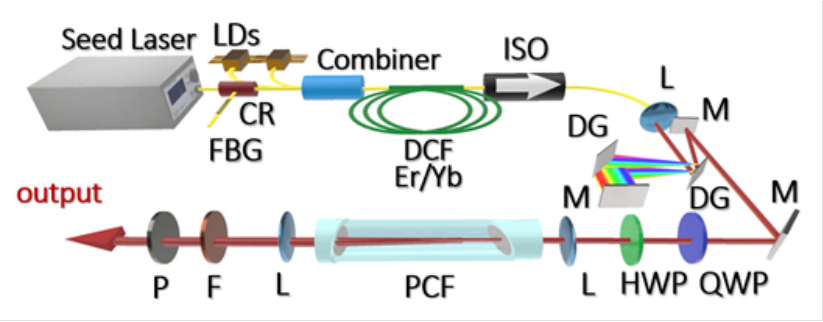

Figure 3. Experimental setup. CR – circulator, LD – laser diodes, L – aspherical lenses, FBG – fiber Bragg-grating stretcher, ISO – isolator, DG – dispersion gratings, M – dielectric mirror, QWP – quarter-wave plate, HWP – half-wave plate, DF – density filter, F – long-pass filter, P – polarizer.

Our experimental setup is schematically shown in Figure 3. The seed laser is a fiber oscillator mode-locked by SESAM. The oscillator output average power of 1.4 mW corresponding to the single pulse energy of 0.13 nJ is achieved at pulse repetition rate of 10.6 MHz. After increasing the average power up to 15 mW in preamplifier, the pulse is stretched from 2 ps to 43 ps duration in the fiber Bragg-grating stretcher. Before the power amplifier, the isolator with a blocked fast axis of polarization sets the linear polarization of the pulse. Finally, the pulse is amplified in the PM double-clad Er/Yb co-doped fiber with a 10-μm core diameter pumped by two high-power 980 nm laser diodes (LD). The maximum output power of the system of 0.6 W is achieved at the pump power of 3.8 W. The pulse from the output of the power amplifier with a duration of about 38 ps is compressed with a pair of diffraction gratings. The linear polarization ensures minimal radiation losses during the compression (less than 5%). Adjusting the distance between the gratings, we reach the compressed FWHM pulse duration of 720 fs at the average output power of ~0.5 W. The spectrum and autocorrelation trace of the compressed pulse recorded by the optical spectrum analyzer Ando AQ-6315E and autocorrelator Femtochrome FL103XL respectively are shown in Figures 4 (a, b). The satisfactory compression quality is evidenced by the fact that the main peak of the gauss fitting contains more than 80% of the pulse energy. The compressed pulse duration is weakly dependent on the output power. As will be seen further, an average output power about 250 mW corresponding to the amplifier output pulse energy of ~ 23.6 nJ and pulse peak power of about ~28 kW is sufficient to shift the Raman soliton to the wavelength of 1700 nm.

After compression, the pulse is launched into the LMA photonic crystal fiber through a special density filter allowing to adjust the input power while other pulse parameters are maintained. The parameters of commercially available PCF-LMA-20 (NKT) correspond to the values shown in the Table 1. The coupling efficiency to the LMA fiber is about 75 %. Figure 4 (a) shows the output spectrum recorded after propagation through the LMA fiber with the length of 1 m the 720 fs pulse with the peak power of ~25 kW (corresponding to the average output power of the amplifier of ~ 220 mW). In this experiment, the pulse polarization is controlled at the amplifier output only and turns to be slightly elliptical at the LMA fiber input. Comparing the Figure 4 (a) with the Figure 1, one can note the typical pattern of N-soliton fission including the generation of Raman soliton. Its spectrum is centered at the wavelength of 1675 nm.

To demonstrate the low-birefringence of the LMA fiber (B = 10-7), we investigate the effect of the polarization rotation on the Raman soliton shift experimentally. Figure 5 shows the spectra of the Raman shifted soliton for different linear polarization states of the launched pulse. The linear polarization of the input pulse is rotated by zero-order half-wave plate. One can see that the change of the input linear polarization has minimal effect on the Raman soliton spectrum confirming the low birefringence of the fiber. Transforming the linear polarization into the circular by the zero-order quarter-wave plate one can observe the similar results, but with the decreased value of the Raman shift. In particular, in

order to achieve the shift to the 1675 nm wavelength the average power of the circularly polarized radiation at the input of the LMA fiber should be raised up to 290 mW corresponding to the increase of pulse energy up to 27.4 nJ.

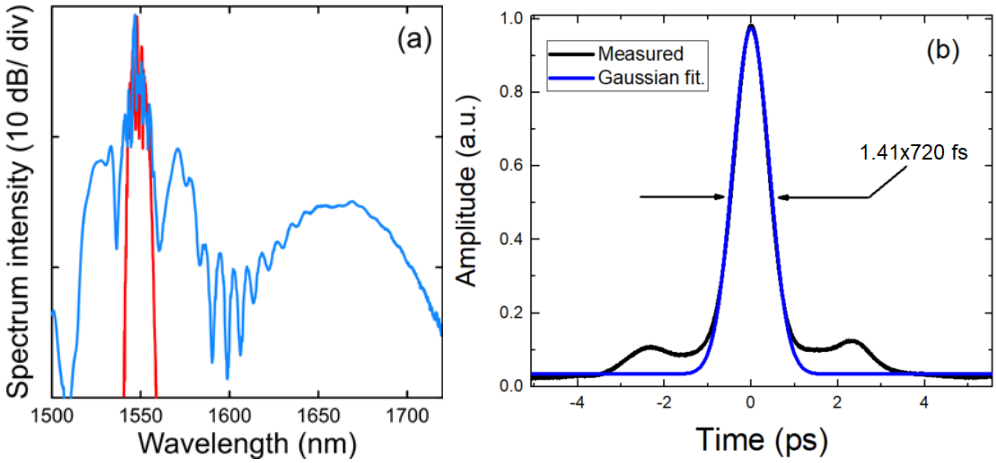

Figure 4. (a) Spectrum of the compressed pulse at the input of the LMA fiber corresponding to the average output power of amplifier ~ 0.5 W (red); spectrum at the output of LMA fiber corresponding to average output power of amplifier ~ 230 mW (blue line). (b) Autocorrelation trace of the compressed pulse at the input of the LMA fiber corresponding to the average output power of amplifier ~ 0.5 W.

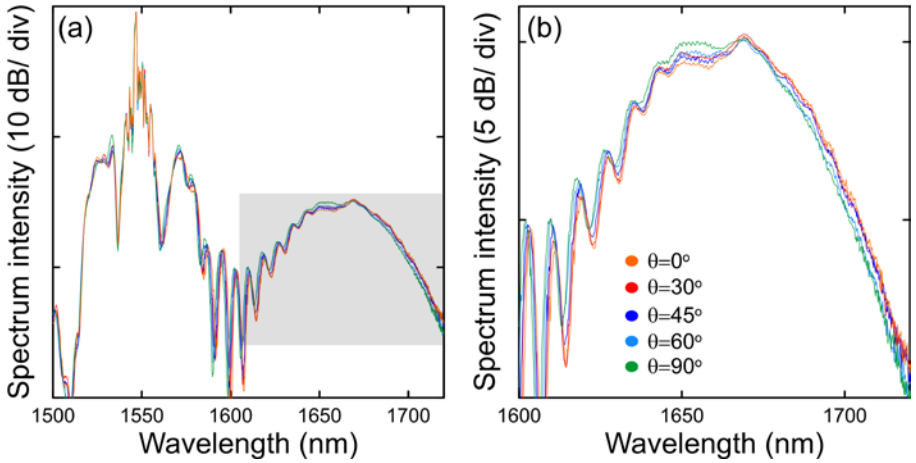

Figure 5. Output spectra for various linear polarization angles θ of the pump pulse measured at the input of the LMA fiber corresponding to the average output power of the amplifier of 220 mW. (a) Output spectra in the range of (1500nm, 1720nm). (b) Enlarged image of the area highlighted in Fig. 5 (a) corresponding to the Raman soliton spectrum.

Next, we experimentally demonstrate the Raman wavelength shift tuning by the control of the polarization of the pulse launched into the LMA fiber, which we considered be-fore numerically. The average power of the radiation at the input of the LMA fiber is fixed at the level of 250 mW corresponding to the pump pulse energy of ~ 23.6 nJ. By rotating the QWP, the polarization of the input pulse can be continuously transformed from linear to circular through a series of intermediate elliptically polarized states. To control the polarization, we used the fast polarization analyzer Keysight N7781B. The polarizer installed at the output of the LMA fiber after the long-pass filter allows us to analyze the polarization of the output radiation component-wise. Figure 6 shows the experimental results of the Raman shift tuning by adjusting the polarization of the input pulse. The spectrum of the output Raman soliton (red line) is the sum of two polarization components: the s- (blue) and the p-component (green), which are measured independently. The average output powers of s- and p- components and the central wavelength λc of the Raman soliton for different polarizations of the input pulse are listed in the Table 2. The total output power after the long-pass filter slightly depends on the state of polarization of the pump pulse indicated by the coloured dot on the Poincare sphere.

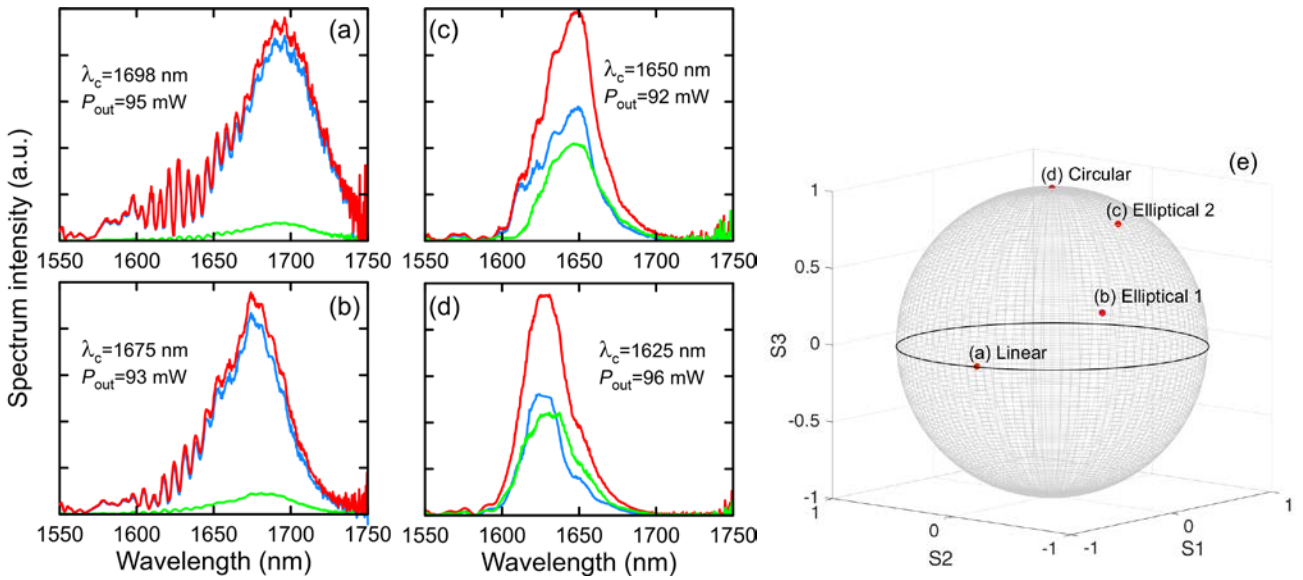

Figure 6. Spectra of s- (blue) and p-polarization component (green) and the sum of two polarizations (red lines) at the output of the LMA fiber after passing the 1600 nm long-pass filter for different polarizations of the input pulse: (a) linear, (b, c) elliptical, (d) circular. Average power at the input of the LMA fiber Pin=250 mW. Pout is the average power at the output of the LMA fiber after the 1600 nm long-pass filter. λc is the wavelength of the spectrum maximum corresponding to the central wavelength of the Raman soliton. (e) States of polarizations of the pump pulse on the Poincare sphere.

Table.2. The average output powers of s- and p- components and the central wavelength λ_c of the Raman soliton for different states of polarization (SOP) of the input pulse.

SOP	$P_{s\ out}$, mW	$P_{p\ out}$, mW	λ_c, nm	SOP	$P_{s\ out}$, mW	$P_{p\ out}$, mW	λ_c, nm
Linear	93	2	1698	Elliptical 2	51	41	1650
Elliptical 1	86	7	1675	Circular	51	45	1625

As one can see, the linearly polarized pump pulse provides the maximum Raman wavelength shift with λc=1698 nm. The polarization of the output radiation passed through the 1600 nm long-pass filter is close to original linearly polarized state. Nearly 98% of the output energy (see Table 2) is retained in the s-component of polarization. Mi-nor excitation of the orthogonal p-polarization we can explain by slight twisting of the LMA fiber. When the polarization state of the input pulse turns to be elliptical, the power of the output p-component grows up but the s-component power lowers, while the total output power passed through the long-pass filter remains almost the same. At the same time, the Raman wavelength shift gradually decreases. When the elliptical polarization is close to circular the s- and p-component output power levels become comparable leading to the minimum Raman shift with λc=1625 nm.

Figure 7 shows the autocorrelations obtained for both polarizations at the output of the LMA fiber after passing the 1600 nm long-pass filter for different polarizations of the pump pulse. (In case of the linear s-polarization of the pump pulse, the output power in p-polarization is insufficient for recording the autocorrelation). One should note that the output autocorrelation is close to autocorrelation of the single Raman soliton but some traces of the pump pulse remainder unabsorbed by the filter can be seen near the main peak. Neglecting the power of the unfiltered pump pulse, we can estimate the energies of the Raman solitons from the data of the Table 2. As one can see, the total energy of the Raman soliton remains almost constant for all the input polarizations amounting to about 9 nJ. In accordance with the simulations, the peak duration corresponding to more powerful polarization component successively decreases when we go from the linear to the circular input pump polarization. The shortest duration of the Raman soliton observed for the linear input polarization is equal to ~60 fs. In this case, a rough estimate of the Raman soliton peak power gives a value of about ~120 kW. Otherwise, for the circular input polarization the main peak duration grows up to ~ 90 fs corresponding to the estimation of the peak power as ~ 40–45 kW for each polarization component. Transition from the linear to the circular input polarization leads to decrease in the distance between the main peak and the pump pulse remainder, which is also in agreement with the simulation results.

Ultimately, we have demonstrated the tuning of the Raman soliton shift in a relatively wide range of 1625-1700 nm by adjusting the polarization of the initial pump pulse at the LMA fiber input. Remarkable property of the proposed

technique is the actual independence of the average output power and energy of the output soliton on the Raman shift wavelength. This feature is highly attractive for a number of applications.

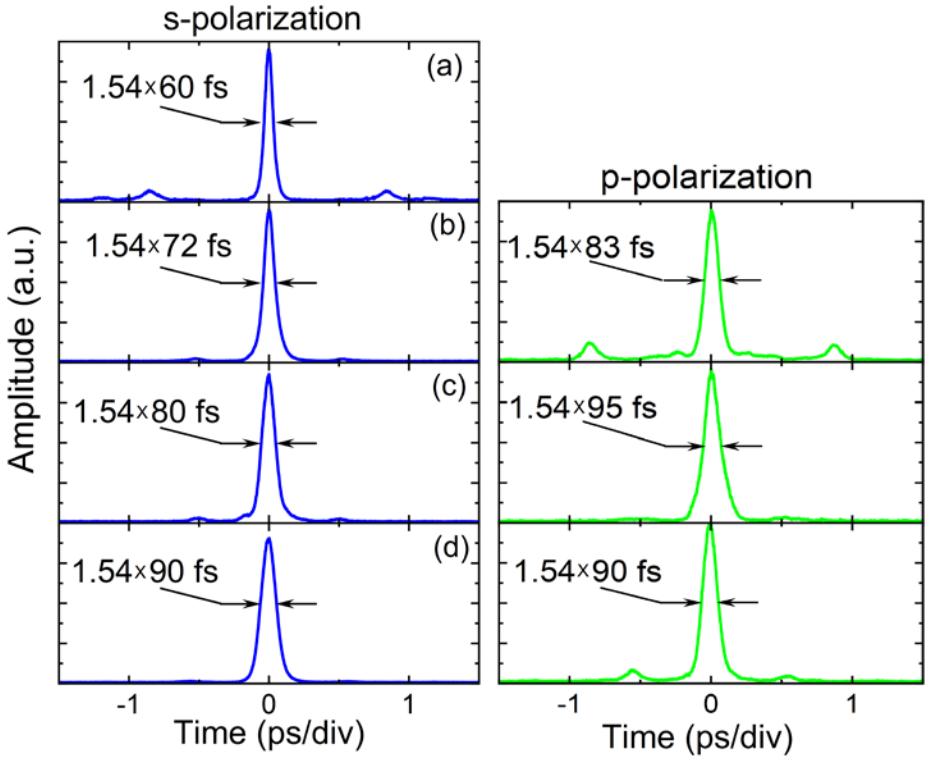

Figure 7. Autocorrelations of s-(blue) and p-polarization (green line) components of the pulse at the output of the LMA fiber after passing the 1600 nm long-pass filter for different polarizations of the input pulse: (a) linear, (b, c) elliptical, (d) circular. States of polarizations of the pump pulse are shown in Figure 6 (e).

4. CONCLUSIONS

Considering the evolution of the sub picosecond pump pulse with the energy of about ~ 20 nJ in the low-birefringent LMA fiber, we numerically investigate the propagation and output parameters of two polarization components of the Raman soliton generated after the pump pulse fission. The simulations show that the final wavelength shift of the Raman soliton depends essentially on the initial state of polarization of the pump pulse. Linearly polarized pump pulse provides the generation of the linearly polarized Raman soliton with the highest peak power and maximum wavelength shift. On the contrary, in the case of circular polarization of the pump pulse, its energy is shared equally between the polarization components leading to the minimum peak power and wavelength shift of the Raman soliton. Thus, by placing the initial state of polarization between these extreme states, it is possible to manage the output wavelength of the Raman soliton without changing of the pump pulse energy.

To test these findings experimentally, the fiber laser setup consisting of the master-oscillator of telecom range, system of chirped pulse amplification (CPA) and compression and low-birefringent output LMA photonic crystal fiber is built. Average output power of the CPA system of about 250 mW is sufficient to obtain the Raman soliton with the energy of ~ 9 nJ. It is shown that the central wavelength of the Raman soliton could be tuned in the range of 1625-1700 nm by adjusting the state of polarization of the pump pulse while the output average power remains nearly constant. The last property is extremely attractive for a number of applications, for example, in the development of multiphoton imaging systems.

The development of fiber laser system is supported by the Ministry of Science and Higher Education of the Russian Federation (project FEUF-2023-0003). Numerical simulations and researches of wavelength tuning are supported by the Russian Science Foundation (project # 22-72-10072).

REFERENCES

[1] Firstov, S., Alyshev, S., Melkumov, M., Riumkin, K., Shubin, A., & Dianov, E., "Bismuth-doped optical fibers and fiber lasers for a spectral region of 1600–1800 nm," Optics letters 39(24), 6927-6930 (2014).

[2] Rivera, V. A. G., El-Amraoui, M., Ledemi, Y., Messaddeq, Y., & Marega Jr, E., "Expanding broadband emission in the near-IR via energy transfer between Er3+–Tm3+ co-doped tellurite-glasses," Journal of luminescence 145, 787-792 (2014).

[3] Chen, S., Jung, Y., Alam, S. U., Richardson, D. J., Sidharthan, R., Ho, D., & Daniel, J. M., "Ultra-short wavelength operation of thulium-doped fiber amplifiers and lasers," Optics express 27(25), 36699-36707 (2019).

[4] Gumenyuk, R., Okhotnikova, E. O., Filippov, V., Korobko, D. A., Zolotovskii, I. O., & Guina, M., "Fiber lasers of Prof. Okhotnikov: review of the main achievements and breakthrough technologies," IEEE Journal of Selected Topics in Quantum Electronics 24(3), 1-14 (2017).

[5] Korobko, D. A., Stoliarov, D. A., Itrin, P. A., Ribenek, V. A., Odnoblyudov, M. A., Petrov, A. B., & Gumenyuk, R. V., "Stabilization of a harmonic mode-locking by shifting the carrier frequency," Journal of Lightwave Technology 39(9), 2980-2987 (2021).

[6] Xu, C., & Wise, F. W., "Recent advances in fibre lasers for nonlinear microscopy," Nature photonics 7(11), 875-882 (2013).

[7] Sordillo, L. A., Pratavieira, S., Pu, Y., Salas-Ramirez, K., Shi, L.; Zhang, L., & Alfano, R. R., "Third therapeutic spectral window for deep tissue imaging," SPIE Optical Biopsy XII 8940, 128-134 (2014).

[8] Spirin, V. V., Escobedo, J. B., Miridonov, S. V., Sánchez, M. M., López-Mercado, C. A., Korobko, D. A., Zolotovskii I.O. & Fotiadi, A. A., "Sub-kilohertz Brillouin fiber laser with stabilized self-injection locked DFB pump laser," Optics & Laser Technology 141, 107156 (2021).

[9] Stoliarov, D. A., Itrin, P. A., Korobko, D. A., Ribenek, V. A., Tabulina, L. V., Sysa, A. V., & Shaman, Y. P., "Saturable absorber based on the fiber coupler coated by CNTs," Optical Fiber Technology 63, 102524 (2021).

[10] Yamanaka, M., Kawagoe, H., & Nishizawa, N., "High-power supercontinuum generation using high-repetition-rate ultrashort-pulse fiber laser for ultrahigh-resolution optical coherence tomography in 1600 nm spectral band," Applied Physics Express 9(2), 022701 (2014).

[11] Geng, J., & Jiang, S., "Fiber lasers: the 2 μm market heats up," Optics and Photonics News 25(7), 34-41 (2014).

[12] Korobko, D. A., Rastogi, V., Sysoliatin, A. A., & Zolotovskii, I. O., "Generation of 2 μm radiation due to single-mode fibers with longitudinally varying diameter," Optical Fiber Technology 47, 38-42 (2014).

[13] Zhluktova, I. V., Kamynin, V. A., Korobko, D. A., Abramov, A. S., Fotiadi, A. A., Sysoliatin, A. A., & Tsvetkov, V. B., "Broadband Supercontinuum Generation in Dispersion Decreasing Fibers in the Spectral Range 900–2400 nm," Photonics 9 (10), 773 (2022).

[14] Sorokina, I. T., Dvoyrin, V. V., Tolstik, N., & Sorokin, E., "Mid-IR ultrashort pulsed fiber-based lasers," IEEE Journal of Selected Topics in Quantum Electronics 20(5), 99-110 (2014).

[15] Ribenek, V. A., Korobko, D. A., Fotiadi, A. A., & Taylor, J. R., "Supermode noise mitigation and repetition rate control in harmonic mode-locked fiber laser implemented through the pulse train interaction with co-lased CW radiation," Optics Letters 47(19), 5236-5239 (2022).

[16] Ribenek, V. A., Stoliarov, D. A., Korobko, D. A., & Fotiadi, A. A, "Pulse repetition rate tuning of a harmonically mode-locked ring fiber laser using resonant optical injection," Optics Letters 46(22), 5687-5690, (2021).

[17] Gumenyuk, R., Korobko, D. A., Zolotovsky, I. O., & Okhotnikov, O. G., "Role of cavity dispersion on soliton grouping in a fiber lasers," Optics express 22(2), 1896-1905 (2014).

[18] Bufetov, I. A., & Dianov, E. M., "Bi-doped fiber lasers," Laser physics letters 6(7), 487 (2009).

[19] Noronen, T., Okhotnikov, O., & Gumenyuk, R., "Electronically tunable thulium-holmium mode-locked fiber laser for the 1700-1800 nm wavelength band," Optics express 24(13), 14703-14708 (2016).

[20] Rissanen, J., Korobko, D. A., Zolotovsky, I. O., Melkumov, M., Khopin, V. F, & Gumenyuk, R., "Infiltrated bunch of solitons in Bi-doped frequency-shifted feedback fibre laser operated at 1450 nm," Scientific reports 7(1), 1-10 (2017).

[21] Filatova, S. A., Kamynin, V. A., Arutyunyan, N. R., Pozharov, A. S., Trikshev, A. I., Zhluktova, I. V., & Tsvetkov, V. B., "Hybrid mode locking of an all-fiber holmium laser," JOSA B 35(12), 3122-3125 (2018).

[22] Dudley, J. M.; & Taylor, J. R. (Eds.), [Supercontinuum generation in optical fibers], Cambridge University Press, (2010).

[23] Chestnut, D. A., & Taylor, J. R., "Soliton self-frequency shift in highly nonlinear fiber with extension by external Raman pumping," Optics letters 28(24), 2512-2514 (2003).
[24] Nishizawa, N., "Generation and application of high-quality supercontinuum sources," Optical Fiber Technology 18(5), 394-402 (2012).
[25] Lopez-Mercado, C. A., Korobko, D. A., Zolotovskii, I. O., & Fotiadi, A. A., "Application of dual-frequency self-injection locked DFB laser for Brillouin optical time domain analysis," Sensors 21(20), 6859 (2021).
[26] Zolotovskii, I. O., Korobko, D. A., Okhotnikov, O. G., Stolyarov, D. A., & Sysolyatin, A. A., "Generation of a broad IR spectrum and-soliton compression in a longitudinally inhomogeneous dispersion-shifted fibre," Quantum Electronics 45(9), 844 (2015).
[27] Lee, J. H., van Howe, J., Xu, C., & Liu, X., "Soliton self-frequency shift: experimental demonstrations and applications," IEEE Journal of Selected Topics in Quantum Electronics 14(3), 713-723 (2008).
[28] Ribenek, V. A., Stoliarov, D. A., Korobko, D. A., & Fotiadi, A. A., "Mitigation of the supermode noise in a harmonically mode-locked ring fiber laser using optical injection," Optics Letters 46(22), 5747-5750 (2021).
[29] Broderick, N. G. R., Offerhaus, H. L., Richardson, D. J., Sammut, R. A., Caplen, J., & Dong, L., "Large mode area fibers for high power applications," Optical Fiber Technology 5(2), 185-196 (1999).
[30] Stutzki, F., Jansen, F., Otto, H. J., Jauregui, C., Limpert, J., & Tünnermann, A., "Designing advanced very-large-mode-area fibers for power scaling of fiber-laser systems," Optica 1(4), 233-242 (2014).
[31] Rehan, M., Kumar, G., Rastogi, V., Korobko, D. A., & Sysolyatin, A. A., "Compression of femtosecond pulses in a wide wavelength range using a large-mode-area tapered fiber," Laser Physics 29(2), 025104 (2019).
[32] Wang, K., Horton, N. G., Charan, K., & Xu, C., "Advanced fiber soliton sources for nonlinear deep tissue imaging in biophotonics," IEEE Journal of Selected Topics in Quantum Electronics 20(2), 50-60 (2013).
[33] Santhanam, J., & Agrawal, G. P., "Raman-induced spectral shifts in optical fibers: general theory based on the moment method," Optics Communications 222(1-6), 413-420 (2003).
[34] Nguyen, T. N., Kieu, K., Churin, D., Ota, T., Miyawaki, M., & Peyghambarian, N., "High Power Soliton Self-Frequency Shift With Improved Flatness Ranging From 1.6 to 1.78 μm," IEEE Photonics Technology Letters 25(19), 1893-1896 (2013).
[35] Korobko, D. A., Ribenek, V. A., Stoliarov, D. A., Mégret, P., & Fotiadi, A. A., "Resonantly induced mitigation of supermode noise in a harmonically mode-locked fiber laser: revealing the underlying mechanisms," Optics Express 30(10), 17243-17258 (2022).
[36] Kato, M., "Wavelength-tunable multicolor Raman soliton generation using an ellipse polarized pump pulse and highly birefringent optical fibers," Journal of lightwave technology 24(2), 805 (2006).
[37] Korobko, D. A., Ribenek, V. A., Itrin, P. A., Stoliarov, D. A., & Fotiadi, A. A., "Polarization maintaining harmonically mode-locked fiber laser with suppressed supermode noise due to continuous wave injection," Optics & Laser Technology 162, 109284 (2023).
[38] Aleshkina, S. S., Fedotov, A., Korobko, D., Stoliarov, D., Lipatov, D. S., Velmiskin, V. V., Temyanko V.L., Kotov L.V.& Likhachev, M. E., "All-fiber polarization-maintaining mode-locked laser operated at 980 nm," Optics letters 45(8), 2275-2278 (2020).
[39] Nishizawa, N., & Goto, T., "Widely wavelength-tunable ultrashort pulse generation using polarization maintaining optical fibers," IEEE Journal of selected topics in quantum electronics 7(4), 518-524 (2001).
[40] Balla, P., & Agrawal, G. P., "Vector solitons and dispersive waves in birefringent optical fibers," JOSA B 35(9), 2302-2310 (2018).
[41] Du, Y., Zhuang, Z., He, J., Liu, H., Qiu, P., & Wang, K., "Self-referenced axial chromatic dispersion measurement in multiphoton microscopy through 2-color third-harmonic generation imaging," Journal of Biophotonics 11(9), e201800071 (2018).
[42] Barad, Y., & Silberberg, Y. R., "Rotating solitons in an isotropic optical fiber," Quantum Electronics and Laser Science Conference, QPD15 (1997).
[43] Tong, S., Chen, X., Li, J., Qiu, P., & Wang, K., "Elliptically-polarized soliton self-frequency shift in isotropic optical fiber," Journal of Lightwave Technology 39(5), 1334-1339 (2021).
[44] Redlich, M. J., Prall, B., Canto-Said, E., Busarov, Y., Shirinyan-Tuka, L., Meah, A., & Lim, H., "High-pulse-energy multiphoton imaging of neurons and oligodendrocytes in deep murine brain with a fiber laser," Scientific Reports 11(1), 7950 (2021).
[45] Lefort, C., "A review of biomedical multiphoton microscopy and its laser sources," Journal of physics D: Applied physics 50(42), 423001 (2017).

[46] Korobko, D. A., Ribenek, V. A., Itrin, P. A., & Fotiadi, A. A., "Birth and annihilation of solitons in harmonically mode-locked fiber laser cavity through continuous wave injection," Optical Fiber Technology 75, 103216 (2023).
[47] Hönninger, C., Plötner, M., Ortaç, B., Ackermann, R., Kammel, R., Limpert, J.,& Tünnermann, A., "Femtosecond fiber laser system for medical applications," SPIE Commercial and Biomedical Applications of Ultrafast Lasers IX 7203, 134-139 (2009).
[48] Perkins, J., Chieffo, L., & Wall, K., "Fiber laser design for biomedical applications," SPIE Optical Fibers and Sensors for Medical Diagnostics, Treatment and Environmental Applications XXIII 12372, 55-59 (2023).
[49] Chen, C. J., Menyuk, C. R., Islam, M. N., & Stolen, R. H., "Numerical study of the Raman effect and its impact on soliton-dragging logic gates," Optics letters 16(21), 1647-1649 (1991).
[50] Menyuk, C. R, Islam, M. N., & Gordon, J. P., "Raman effect in birefringent optical fibers," Optics letters 16(8), 566-568 (1991).
[51] Rao D.S., Karpate, T., Ghosh, A. N., Gonzalo, I. B., Klimczak, M., Pysz, D., Dudley J. & Sylvestre, T., "Noise in supercontinuum generated using PM and non-PM tellurite glass all-normal dispersion fiber," Optics Letters 47(10), 2550-2553 (2022).
[52] Ghosh, A. N., Meneghetti, M., Petersen, C. R., Bang, O., Brilland, L., Venck, S., & Sylvestre, T., "Chalcogenide-glass polarization-maintaining photonic crystal fiber for mid-infrared supercontinuum generation," Journal of Physics: Photonics 1(4), 044003 (2019).